Cold Regions Science and Technology 59 (2009) 202–209

Contents lists available at ScienceDirect

Cold Regions Science and Technology

journal homepage: www.elsevier.com/locate/coldregions

Quantifying changes in weak layer microstructure associated with artificial load changes

Eric Lutz [a,b,*], Karl Birkeland [a,c], Hans-Peter Marshall [d,e]

[a] Department of Earth Sciences, Montana State University, Bozeman, MT, 59717, United States
[b] Civil and Environmental Engineering, University of Washington, Seattle, WA, 98195-2700, United States
[c] USDA Forest Service National Avalanche Center, Bozeman, MT, United States
[d] Center for Geophysical Investigation of the Shallow Subsurface, Boise State University, Boise, ID, United States
[e] Cold Regions Research and Engineering Laboratory, Hanover, NH, United States

ARTICLE INFO

Article history:
Received 7 November 2008
Accepted 20 April 2009

Keywords:
Snow microstructure
Stability
Loading event
Elastic rebound
SnowMicroPen

ABSTRACT

Researchers and practitioners have long utilized a variety of penetrometers to investigate the snowpack. Identifying definitive relationships between penetrometer-derived microstructural information and stability has been challenging. The purpose of this study is two-fold: 1. We propose a simple field test to establish relationships between load and penetrometer-derived microstructural estimates, 2. We utilize the SnowMicroPen (SMP) to quantify changes in weak layer residual strength and microstructural dimension associated with an artificial loading event. Our dataset is from Moonlight Basin, Montana and includes three modified loaded-column tests, each paired with 5 SMP profiles. Depth hoar comprised the targeted weak layer. Results indicate that loading caused the residual strength and rupture frequency to decrease significantly. Much like a compression test at a micro-scale, the force required for the SMP to rupture individual structures as well as the micro-scale strength decreased significantly when the slab stress was increased by artificially adding blocks of snow. A decrease in observed rupture frequency within the weak layer (or an increase in the distance between ruptured structures) also occurred after the loading event, probably because some structures within the weak layer had already failed or were so close to failing that the penetrometer could not detect their rupture. Due in part to the large difference in loads, microstructural differences between the natural and loaded columns were significant enough that only one profile would have been necessary to determine a significant difference in residual strength. Artificial removal of slab stress resulted in greater rupture forces and larger microstructures, likely due to elastic rebound.

1. Introduction

Snow hardness has long been recognized as an important proxy for determining the structure and strength of mountain snowpacks (Bader et al., 1939). Researchers have developed a variety of penetrometers–ranging from manual to mechanical to digital–with the long-term goal of efficiently and objectively deriving stability information from resistance profiles (e.g. Bader et al., 1939; DeQuervain, 1950; Bradley, 1966; Dowd and Brown, 1986; Brown and Birkeland, 1990). In the late 1990's, Schneebeli and Johnson developed the SnowMicroPen (SMP) to record penetration resistance at force and stratigraphic resolutions that enable grain and bond-scale strength properties to be estimated (Schneebeli and Johnson, 1998; Johnson and Scheebeli, 1999; Schneebeli et al., 1999).

Previously published SMP field studies have measured natural instabilities of undisturbed snow. Opportunities to test instabilities related to loading events are limited in a given season and region by: (1) the presence of weak layers, (2) the number of critical loading events, (3) the logistical challenges of timing field campaigns to precede and coincide with a loading event and, (4) the real possibility of collapsing the weak layer when approaching the site and while sampling. In part because of these factors, direct correlations between penetration hardness, micro-structural estimates, and snowpack strength and stability have proven challenging (Birkeland et al., 2003; Kronholm, 2004; Lutz et al., 2007; Pielmeier et al., 2006). Developing relationships between loading events and resultant changes in microstructure will require many different types of instabilities to be examined.

In this study we decreased snowpack stability by artificially loading an existing weakness using a modified loaded column test. The loaded column test, also referred to as a collapse test, quantifies how large of a static load (or overburden) is needed to cause fracture of the weakest stratigraphic feature within an isolated column of snow (McClung and Schaerer, 1993). Because blocks of snow are statically added over a period of minutes until fracture occurs, the loading process is more rapid than a natural snowfall event and much slower than dynamic skier-loading. Fuller (2004) conducted field-based strain experiments on isolated columns using a dial gauge and was able to observe deformation

* Corresponding author. Civil and Environmental Engineering, University of Washington, Seattle, WA, 98195-2700, United States. Tel.: +1 406 599 2107.
E-mail addresses: snowscience@gmail.com, e_lutz@mac.com (E. Lutz).

0165-232X/$ – see front matter © 2009 Elsevier B.V. All rights reserved.
doi:10.1016/j.coldregions.2009.04.003

and elastic rebound for a range of artificial loads and load durations. The loaded column test has been recognized by practitioners as a useful tool for estimating the approximate precipitation load needed to cause failure (Greene et al., 2004).

The forced instability was then recorded with the SMP and the snowpack's micro-scale residual strength under the applied overburden was estimated. By additionally recording SMP profiles in column tests with natural and reduced slab loads, we could identify how microstructural properties of stratigraphic features changed under different load conditions.

2. Methods

2.1. Study area and snowpack

On 28 March 2008, we collected field data at Moonlight Basin's Corner Pocket where depth hoar subsisted under an ice crust and wind slab. The weakest depth hoar layer was approximately 10 cm thick, with a series of thick crusts and dense depth hoar below. The targeted layer consisted of well-preserved depth hoar crystals, ranging from 6 to 10 mm in length, aggregated in 10–30 mm columns (5dh, Colbeck et al., 1990). A temperature gradient of 8 °C·m^{-1} existed within the upper 5 cm of depth hoar (directly under the slab). The thick (2 cm) crust directly above the depth hoar consisted of small (<0.5 mm) mixed forms (3c, Colbeck et al., 1990). At the study site, the weak layer was buried below a slab containing approximately 193 mm water equivalent. No single, large loading event preceded our observations; the Moonlight Ski Patrol reported that several small snowfall events cumulatively deposited 39 mm water equivalent over the 10 preceding days.

2.2. Field method

Observations included three modified loaded column tests, each paired with five SMP profiles (grey dots in Fig. 1, left). The three columns were isolated on their front and sides so that the 10 cm thick weak layer was exposed at the base. Column II's unaltered slab represented the natural load. To determine approximately how much additional snow was needed to cause fracture, we performed a practice loaded column test. Then we loaded Column III with slightly less snow than was applied in the practice test, using blocks from the top of Column I and additional blocks, bringing the weak layer close to fracture. After isolating the backside of the columns, we made SMP measurements into the lower portion of the columns.

Since the columns were situated on an inclined slope and the SMP is generally driven perpendicular through stratigraphy, the operator drove the probe obliquely through the face of the columns, carefully positioning the SMP close to the columns without unintentionally scraping the bipod legs on the column corners (Fig. 1, right). Further, care must be taken to ensure that the SMP does not probe near the column edges. With 5 SMP profiles per column, we were able to maintain about 10 cm distance from the column edges. We recorded SMP measurements in sets of three, one in each column (first set of three SMP measurements are denoted with numbers and arrows in Fig. 1). This sequence allowed the examination of changes occurring in any column during the sampling duration of approximately 35 min.

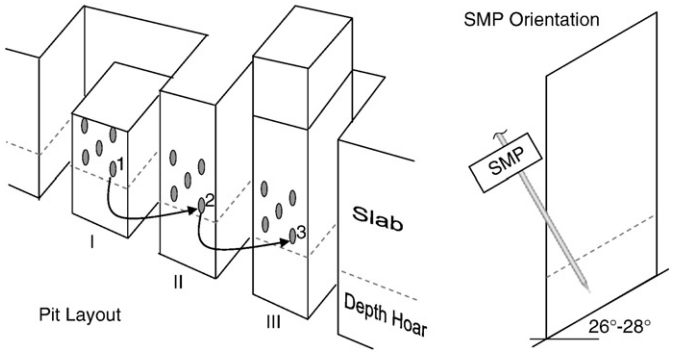

Fig. 1. Pit sample layout. We isolated three 30 cm × 30 cm columns with different loads (I, II, and III) and recorded weak layer strength with the SMP. One set of SMP profiles included a profile from each column (arrows).

After completing SMP measurements we dynamically loaded each column until fracture, using standard compression test (CT) force loads (Greene et al., 2004). While the observed CT values provide additional stability information, the SMP probe holes likely affected the test results for all columns. After failure, we vertically sectioned and placed each column into a large nylon bag and weighed them using a large spring scale, eliminating the need for time-consuming density measurements to calculate slab stress. For each column, the associated slab stresses were calculated by dividing the slab loads by the surface area of an isolated column (0.09 m^2). Because the column dimensions were measured to an accuracy of 1 cm, the surface area of the isolated columns at the weak layer fracture location may have varied by ±0.006 m^2. Maximum error limits were calculated for slab stresses and stress differences between adjacent columns (including hypothetical situation where adjacent columns have opposite errors). We assumed that the slope angle of the fracture plane was the same as that of the snowpack surface.

2.3. Delineation of slab–depth hoar transition

To compare microstructural estimates from adjacent layers (i.e. superstratum and weak layer) and from adjacent columns, in each SMP profile we delineated the transition between the ice crust at the bottom of the slab and the depth hoar manually, which is typical for SMP research (e.g. Birkeland et al., 2003). Every SMP profile exhibited the interface of interest, observed as an abrupt decrease in mean resistance and increase in local variance. Profile depth was set to zero at this interface.

2.4. Microstructural estimates

We derived three microstructural properties of the superstratum–weak layer complex from rupture size and frequency information recorded within SMP profiles. Sharp drops in the force–distance record were interpreted as individual structural elements rupturing. It was unknown whether a given fracture occurred at a bond location, or in the middle of an element. In either case, the rupture was assumed to be associated with an individual structural element. For a profile segment of length z (mm), the mean rupture force normal to sensor tip f (N) is the sum of the rupture values divided by the number of ruptures N, and corrected for the cone tip angle. As defined by Johnson and Schneebeli (1999) the structural element length L (mm) can be derived from N and the volume of snow sampled, such that

$$L = 3\sqrt{\frac{\pi r^2 z}{N}}$$

where r is equal to the radius of the sensor tip. Lastly, by dividing f by L^2 we estimated the micro-scale strength σ_{micro} (N·mm^{-2}) which describes a potential relationship between strength and structure (Johnson and Schneebeli, 1999).

Instrumental noise was eliminated by applying noise thresholds before calculating these microstructural estimates. A noise threshold was defined for each SMP profile independently, by calculating the 98th percentile of drop values recorded in the air signal above the snow surface. This technique may be better than using a single threshold for multiple profiles because noise in adjacent SMP profiles

Table 1
Compression test field observations.

Property	Column		
	I	II	III
Description	Reduced load	Natural load	Increased load
Slab mass (kg)	8.1	15.4	25.8
Slope angle (°)	26.5	27.5	28
CT score	23	20	5
Shear quality	2	2	1

varies even in high quality data. In this dataset the threshold value varied between 0.025 N and 0.030 N, with a median value of 0.029 N. No profiles contained obvious low quality signal characteristics such as artificial dampening or trends, as described by Lutz (2009).

We applied Marshall and Johnson's (submitted for publication) micromechanical model, which modifies Johnson and Schneebeli's (1999) model by accounting for limitations of the one-dimensional force signal, its force and depth resolution, and removing assumptions of constant mechanical properties within the region influencing the SMP measurement. Marshall and Johnson (submitted for publication) found the modifications improve the accuracy of microstructural estimates, and all modifications were necessary to achieve accurate inversion results in extensive simulations, over the entire range of micromechanical properties observed in natural snow. The modifications relevant to calculating f, L and σ_{micro} account for simultaneous ruptures and correct for a force digitization error at rupture.

2.5. Moving-window application of estimates

Microstructural estimates were calculated from 5 mm profile segments. Each profile provided 20 weak layer samples and 5 slab samples, each derived from independent (non-overlapping) 5 mm signal segments. The number of slab samples was limited because SMP profiles contained only the base of the slab. The transition between the slab and weak layer was excluded from both sample groups. For each SMP profile, the stratigraphic step-changes Δf, ΔL and $\Delta\sigma_{\text{micro}}$ were calculated by subtracting the median of the 20 weak layer samples from the median of the 5 slab samples. Results from the slab properties were used to derive step-changes but are not otherwise analyzed in this manuscript. Since each isolated column contained 5 SMP profiles, each column provided 5 step-change values of Δf, ΔL and $\Delta\sigma_{\text{micro}}$, 100 weak layer samples of f, L, and σ_{micro}, and 25 slab samples of f, L, and σ_{micro}.

2.6. Analysis

The non-parametric Wilcoxon Test quantitatively tested for differences in centrality of microstructural properties (1) between adjacent columns (2) between individual profiles from different columns, and (3) between individual profiles from the same column. While the first comparison allowed for general differences between columns to be identified, the second enabled us to test the effectiveness of individual profiles at identifying the same general differences found in the first comparison type. The last comparison helped determine if a time-effect is evident over the sampling period.

Figs. 3, 5, and 7–9 use boxplots to show the distributions of estimated microstructural parameters. These figures visualize changes in microstructural properties and contain graphical features that illustrate statistical properties of each group as well as relationships between adjacent groups. Black squares represent median values, whiskers represent the range, and the top and bottom limits of boxes delineate the inter-quartile range. Triangles on the sides of boxes represent approximate 95% non-parametric confidence intervals of the mean (McGill et al., 1978; Chambers et al., 1983), as applied by the *R* function *boxplot.stats*. In our application, the triangle color is used to indicate a significant (white) or insignificant (grey) difference in median values between adjacent groups, tested by the Wilcoxon Rank Sum Test, and assuming a 95% confidence level. Bracketed values represent the number of sampled 5 mm segments.

3. Results and discussion

3.1. Compression tests

Compression test (CT) scores reflected the load differences (Table 1). The weak layer under the artificially reduced slab (Column I) scored slightly higher CT values than did Column II. Column III fractured at a much lower loading step than the other columns and it also produced a Quality 1 shear (Table 1). Based on these observations, we characterized Column I and II as "stable" and Column III as "unstable". Fractures occurred within the weak layer between 2 and 5 cm of the slab–weak layer interface. This was estimated by observing the amount of intact depth hoar still attached to the slab after fracture.

3.2. Slab stress (Pa) and micro-stress ($N \cdot mm^{-2}$)

Artificial changes in slab thickness caused slab stress to vary dramatically between the three columns (Part 1 of Table 2). Compared

Table 2
Slab stress (Part 1), SMP-derived microstructural estimates of the weak layer (Part 2) and associated step-changes (Part 3), for test columns I through III.

Property	Columns			Change:		Change:	
	I	II	III	Natural → unloaded		Natural → loaded	
	Unloaded	Natural	Loaded	Col. I–Col. II		Col. III–Col. II	
Part 1. Slab stresses				Δ	*|Error limits|*	Δ	*|Error limits|*
Shear (Pa)	3.93e + 02	7.73e + 02	1.32e + 03	−3.79e + 02	*|−3.03e + 02 −−4.59e + 02|*	5.48e + 02	|4.10e + 02–6.89e + 02|
Normal (Pa)	7.88e + 02	1.48e + 03	2.48e + 03	−6.96e + 02	*|−5.46e + 02 −−8.50e + 02|*	9.99e + 02	|7.37e + 02–1.27e + 03|
Vertical (Pa)	8.80e + 02	1.67e + 03	2.81e + 03	−7.92e + 02	*|−6.24e + 02 −−9.65e + 02|*	1.14e + 03	|8.43e + 02–1.44e + 03|
Part 2. Microstructural estimates of weak layer				Δ	(*p*-value)	Δ	(*p*-value)
f_{median} (N)	2.08e-01	1.89e-01	1.37e-01	**1.90e-02**	***(3.69e-02)***	**−5.16e-02**	***(8.88e-16)***
L_{median} (mm)	1.11e + 00	1.07e + 00	1.37e + 00	**3.74e-02**	***(6.20e-03)***	**2.97e-01**	***(1.31e-25)***
$\sigma_{\text{micro median}}$ ($N \cdot mm^{-2}$)	1.68e-01	1.64e-01	7.53e-02	4.20e-03	*(8.71e-01)*	***−8.87e-02***	***(<0.00e-16)***
Part 3. Step-change of microstructural estimates				Δ	*p*-value	Δ	*p*-value
Δf_{median} [(N)]	−2.89e-01	−2.73e-01	−2.10e-01	−1.60e-02	*(1.00e + 00)*	6.38e-02	*(1.44e-01)*
ΔL_{median} (mm)	3.75e-01	3.21e-01	5.26e-01	5.38e-02	*(5.31e-01)*	**2.06e-01**	***(1.22e-02)***
$\Delta\sigma_{\text{micro median}}$ ($N \cdot mm^{-2}$)	−7.94e-01	−7.65e-01	−4.79e-01	−2.88e-02	*(6.76e-01)*	2.86e-01	*(4.03e-01)*

Italicized numbers in Part 1 show maximum possible stress errors, considering column dimensions were measured to an accuracy of 1 cm.
For slab micro-stresses ($N \cdot mm^{-2}$), multiply values in Part 1 by 1×10^{-6}. Italicized numbers in Parts 2 and 3 are *p*-values from the Wilcoxon Test, indicating whether a significant ($p = 0.05$) difference in central tendency existed between two columns. Significant differences are in bold.

with Column II, Column I had an artificial vertical load reduction of approximately 792 Pa (limits due to maximum possible measurement error: 624–965 Pa) and Column III experienced an artificial vertical load increase of approximately 1140 Pa (limits due to maximum possible measurement error: 843–1440 Pa). To compare the slab stresses with SMP-derived micro-scale strength estimates (Section 3.3), we converted the slab stresses (Pa) to micro-stresses ($N \cdot mm^{-2}$) by multiplying the stresses by 1×10^{-6}.

Since the load-altered columns were within 30 cm of the unaltered column, possessed similar slope angles, and original slab thickness did not vary by more than 1 cm between adjacent columns, the difference in observed applied stress was considered to be the result of the artificial changes rather than spatial variability. We can contextualize the degree that a 1 cm difference of slab thickness might have influenced slab load at initial conditions. If this difference existed within a denser portion (e.g. 300 kg m^{-3}) of the slab, then the slab load of adjacent columns at initial conditions would differ by 29.4 Pa, which for the isolated columns would equate to a slab mass difference of 0.27 kg. We consider this amount of variation at initial conditions negligible, since it nears the accuracy limit of the scale and measurement technique and because it is significantly smaller than the observed loads and load differences.

3.3. Changes in weak layer microstructural estimates

In the weak layer, f was significantly smaller under the artificial load than it was under the natural load; on average the SMP ruptured structures with 0.052 N less force when we increased the overburden on the weak layer (Part 3 of Table 2; Figs. 2 and 3). When we consider the differences in distributions evident in Fig. 3, a f split-value of 0.158 N successfully differentiated 75.5% of observations, whereby 69% of Column III's samples are differentiated from 82% of the samples from Column II (horizontal black dotted line in Fig. 3). A classification accuracy of 70.5% was obtained when a threshold between 0.130 and 0.183 N was selected (grey horizontal bar in Fig. 3). This indicates that in this dataset f differentiated most of the unstable samples from the stable samples in column II. Based on this observation, f may prove useful for characterizing changes in weak layer strength and snowpack stability.

Column I possessed significantly higher mean rupture forces than Column II, with an average difference of 0.019 N. We interpret this difference as an increase in residual strength related to elastic rebound. Removing a large portion of the natural slab (in this instance, a stress reduction of approximately 792 Pa) may allow the structures to recover the elastic component of the deformation caused by the slab, to a less stressed (and strained) state. Under this new circumstance, slightly more force would be required for the SMP to rupture these structures because they are under less stress, resulting in slightly higher measured rupture forces. In nature this could relate to increases in stability directly following wind scour events.

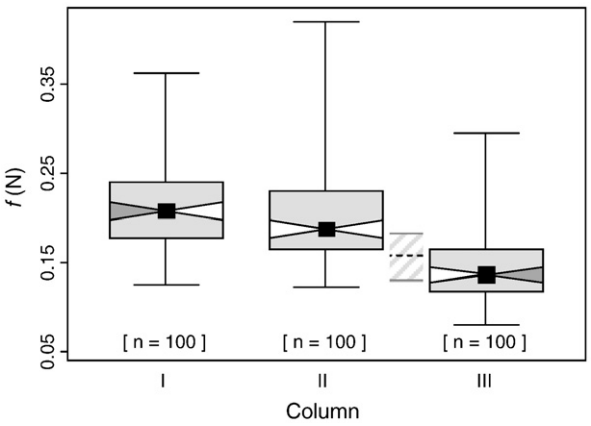

Fig. 3. Mean rupture force f of weak layer. The unloaded column (I) possessed the highest average f values and the loaded column (III) maintained the smallest values. Horizontal dashed line at 0.158 N represents threshold value with maximum accuracy (75.5%) and cross-hatching delineates split-values with at least 70.5% accuracy.

Within the weak layer, L was significantly greater under the artificially loaded column than under the natural load; on average, L was 0.3 mm greater (Part 3 of Table 2; Figs. 4 and 5). L accurately differentiated 81.5% of the unstable and stable samples when a split-value between 1.12 and 1.26 mm was selected (Fig. 5). A maximum accuracy of 86.5% was obtained using a split-value of 1.15 mm, which differentiated 95% of the unstable samples from 78% of the stable samples from Column II (Fig. 5). Lutz (2009) identified similar changes in L associated with a natural loading event. We hypothesize that, under the increased load, some structures within the weak layer have begun to fail or are so close to failing that we cannot differentiate their rupture from instrumental noise, resulting in fewer observable ruptures within a given distance, and an increase of L. Since ruptures occur when either bonds between structural elements or the structures themselves fracture, the volumetric density of bonds and intact structures appears to have been reduced under the artificial load. This support previous research that identified bond density as well as the structural element length, or "fundamental unit" as

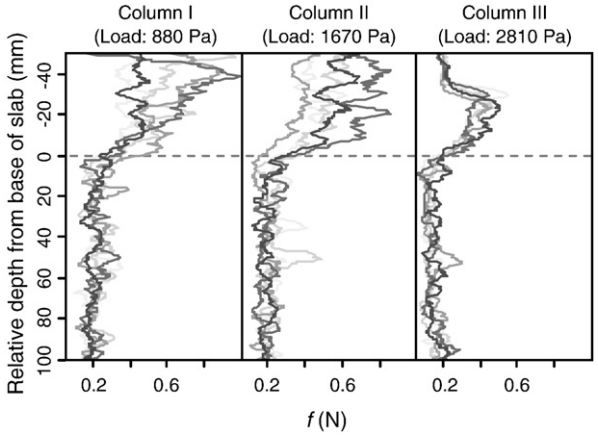

Fig. 2. Profiles of the mean rupture force f indicate that the smallest f occurs within the depth hoar and coincides with the greatest overburden (Column III). Horizontal line approximates the upper boundary of the targeted depth hoar layer. Lines of different shades of grey represent different SMP profiles. Note that the slab also becomes weaker in Column III.

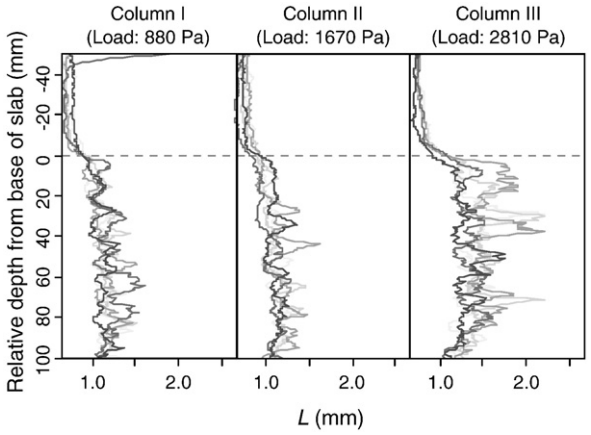

Fig. 4. Microstructural element length L was consistently greater in the depth hoar than in the slab, and was greatest under the artificial load (Column III). Horizontal line approximates the upper boundary of the targeted depth hoar layer. Lines of different shades of grey represent different SMP profiles.

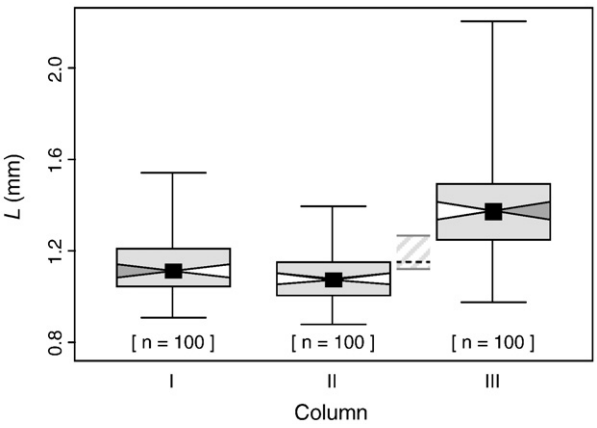

Fig. 5. Microstructural element length *L*. The loaded column (III) possessed the highest *L* values and the natural column (II) maintained the smallest *L* values. Horizontal dashed line at 1.15 mm represents threshold value with maximum accuracy (86.5%) and cross-hatching delineates split-values with at least 81.5% accuracy.

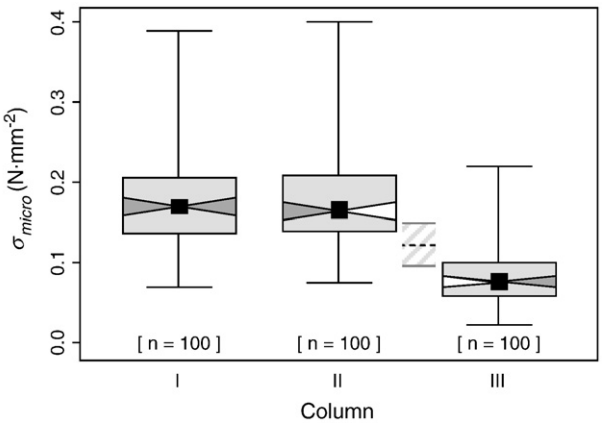

Fig. 7. Micro-scale strength σ_{micro} of weak layer. The loaded column (III) possessed the lowest *S* values while the unloaded and natural columns (I and II) were indistinguishable. Horizontal dashed line at 0.118 $N \cdot mm^{-2}$ represents threshold value with maximum accuracy (86.5%) and cross-hatching delineates split-values with at least 81.5% accuracy.

described by Gubler (1978), as determinants of stability (Yosida et al., 1956, in Shapiro et al., 1997; Gubler, 1978; Schweizer, 1999).

Interestingly, a small but significant increase in *L* occurred when the slab stress was artificially reduced, as evident from Column I (Part 3 of Table 2; Figs. 4 and 5). Since stress was removed from this column, and *f* increased, it is possible that this increase in *L* was a direct result of elastic rebound. Hence, the change in *L* may be representative of stored strain energy (Mellor, 1975). A direct relationship between the SMP-derived microstructural estimates and bulk elastic rebound can be further explored by coupling isolated column tests with SMP and strain gauge measurements such as those described by Fuller (2004). This may allow for relationships to be established between SMP-derived estimates and rheological models, such as Burgers model (Maxwell and Kelvin–Voigt models in series), that have been used to describe elastic stress dissipation observed in cold lab studies (Mellor, 1975; Shapiro et al., 1997).

σ_{micro} was significantly smaller under the increased load on Column III (Figs. 6 and 7). σ_{micro} decreased by 8.87×10^{-2} $N \cdot mm^{-2}$ when vertical micro-stress increased by 1.14×10^{-3} $N \cdot mm^{-2}$. No statistically significant change of σ_{micro} occurred when the vertical micro-stress decreased by 7.29×10^{-4} $N \cdot mm^{-2}$. This shows us that if *f* decreases and *L* increases, as observed for the loaded column, σ_{micro} becomes small, which we would expect. If, on the other hand, *f* and *L* both increase, σ_{micro} does not change significantly because the higher residual strength is distributed over slightly larger structure lengths (or fewer structures and bonds per volume). σ_{micro} may prove very useful in characterizing changes in weak layer strength and snowpack stability (Fig. 7). Examining a natural instability, Lutz (2009) identified significant changes in σ_{micro} associated with a snowfall event.

At least 81.5% of the unstable and stable samples could be accurately differentiated when a σ_{micro} split-value was selected between 0.092 and 0.145 $N \cdot mm^{-2}$. A maximum accuracy of 86.5% was obtained using a split-value of 0.118 $N \cdot mm^{-2}$, which differentiated 90.5% of the unstable samples from 82.5% of the stable samples of Column II (Fig. 7). This indicates that σ_{micro} alone very effectively distinguished the loaded weak layer from the natural weak layer. The micro-scale strength σ_{micro} distinguished Column III data (unstable, CT = 5) from Column I and II data (stable, CT = 23, 20) with much more accuracy than *f* and *L* alone. Using a large dataset of Rutschblock tests paired with multiple SMP profiles, Pielmeier and Marshall (2009-this issue) found σ_{micro} to be the most significant in classifying Rutschblock (RB) stability, using a σ_{micro} classification threshold value of 0.10 $N \cdot mm^{-2}$.

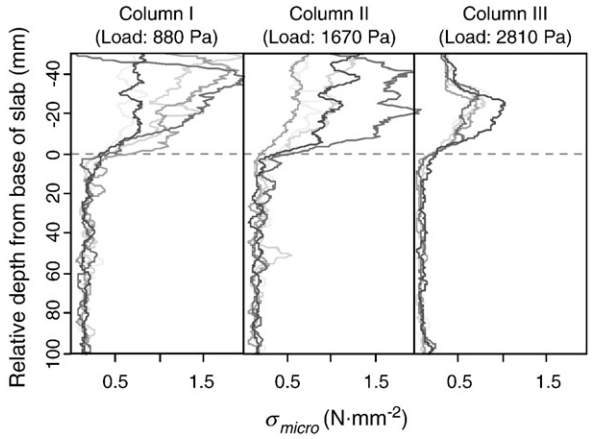

Fig. 6. Micro-scale strength σ_{micro} was smaller within the depth hoar than in the slab and was smallest under the artificial load (Column III). Horizontal line approximates the upper boundary of the targeted depth hoar layer. Note that the slab also becomes significantly weaker in Column III.

3.4. Effectiveness of individual SMP profiles at identifying changes due to loading event

This analysis focused on the two columns representing natural and loaded slab conditions. Because each profile contained 20 weak layer samples, it was possible to treat each individual profile as its own statistical distribution and test how effective individual SMP profiles were at discerning a significant change in stability between the natural and loaded columns. The profile-based Wilcoxon Tests revealed that, of the 25 possible comparisons between individual SMP profiles from the unstable column (III) with those from the stable column (II), 23 tests (92%) indicated significant decreases in *f*, and all

Table 3
Count and percentage of profile comparisons yielding results that are representative of the column results involving the natural column (II) and the loaded column (III).

Expected change due to loading (based on column comparisons in Part 3 of Table 2):	Was the expected change observed in profile comparisons?	
	Yes	No
	Count (%)	Count (%)
Significant ↓ of *f*	23 (92%)	2 (8%)
Significant ↑ of L	25 (100%)	0 (0%)
Significant ↓ of S	25 (100%)	0 (0%)

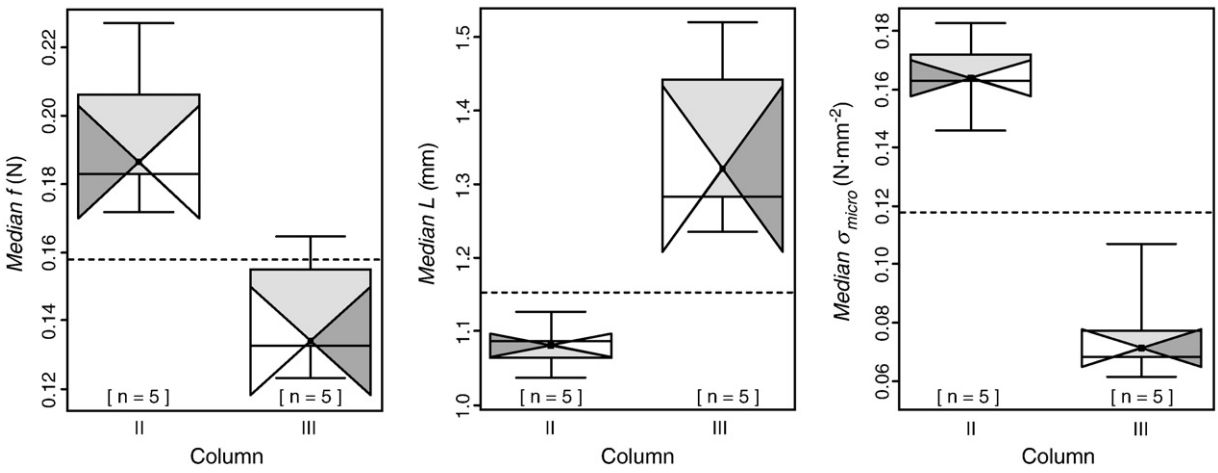

Fig. 8. Boxplots of the median values of microstructural estimates for the natural (II) and loaded (III) columns. Each boxplot contains 5 median values, each derived from 20 samples from a given SMP profile. Dashed horizontal lines represent the threshold value with maximum classification accuracy (Section 3.3). Note that for both columns, median values of L and σ_{micro} are clearly differentiated by these threshold values. The confidence intervals are larger than the inter-quartile ranges due to the small sample sizes.

25 tests (100%) indicated significant increases of L and significant decreases of σ_{micro} associated with the artificial loading (Table 3).

In addition to these statistically significant relative differences between profiles originating from Columns II and III, each profile's median value (derived from 20 available samples) in these two columns consistently placed on the expected side of the previously described split-value of 0.118 N for σ_{micro} (Fig. 8). This means that for this field study only one profile would be necessary per column to identify that a significant decrease in micro-scale strength occurred in the artificially loaded column and that the median σ_{micro} value for each profile was successfully used to classify each profile to column II or III, when a σ_{micro} threshold value of 0.118 N was applied. This high degree of representativity would not be expected for thin weak layers, where less microstructural information is recorded, or for smaller loading events that produce smaller changes in microstructural estimates. These more subtle conditions are examined by Lutz (2009).

3.5. Time-effect of loading on weak layer properties

No changes were evident in micro-scale strength σ_{micro} of Columns I and II. However, in Column III σ_{micro} increased significantly over the 35-min sampling duration (Fig. 9), mainly due to a decrease of L. This indicates that distances between structures became smaller. This could be due to bonds or contact points regaining strength (sintering) or due to plastic deformation over the sampling period resulting in more tightly spaced structures. In either case, at the micro-scale, some amount of strengthening appears to have occurred in Column III associated with the decrease of L.

This interpretation requires caution however, since adjacent profiles may have affected the microstructure within a given column.

3.6. Step-changes of microstructural estimates

The difference in L between the weak layer and adjacent slab, described by ΔL, was significantly larger under the artificially loaded slab than under the other loads (Part 4 of Table 2, and Fig. 10). A similar association between ΔL and stability was observed by Pielmeier et al. (2006) and Pielmeier and Schweizer (2007). In this study the increase in ΔL under the unstable column was a direct result of L increasing more in the weak layer than it did in the adjacent slab. This supports the general assertion that stratigraphic features containing fewer or weaker structures are more susceptible to changes in stress (Shapiro et al., 1997).

There appears to be a decrease in the step-changes Δf and $\Delta\sigma_{\text{micro}}$, which might indicate that under the artificial load the stratigraphic

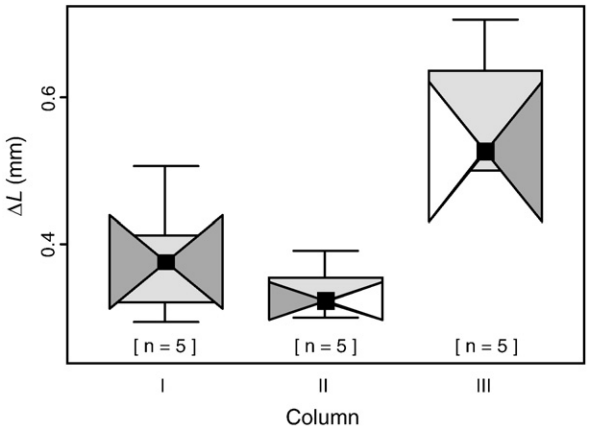

Fig. 9. Weak layer micro-scale strength σ_{micro} of Column III, grouped by sample (SMP profile) order (approximately 8 min between profiles). The confidence intervals are larger than the inter-quartile ranges due to the small sample sizes.

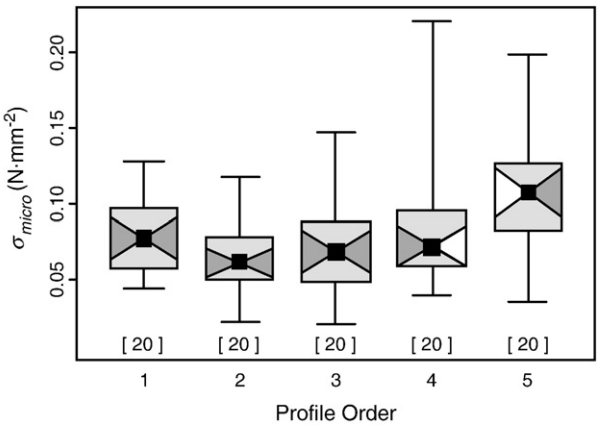

Fig. 10. Stratigraphic step-change of the structural element length, ΔL, had positive values for all three columns, indicating that the weak layer consistently had larger L values than the adjacent slab. The loaded column (III) had a significantly larger ΔL value than the other two columns. Confidence intervals overlap hinges because of small sample sizes.

differences in f and σ_{micro} may became smaller (Part 4 of Table 2). However, these changes are insignificant, possibly due to the small sample sizes ($n=5$).

4. Conclusions

4.1. Observed Phenomena

The findings indicate that distinct differences in L, f, and σ_{micro} existed in the weak layer under different loads. Increasing stress by adding an artificial load caused f and σ_{micro} to decrease, and L to increase. Viewed over a short time window, L decreased slightly which may be evidence of strengthening.

Decreasing slab stress by removing much of the natural slab coincided with slight increases in f and L. While the overall micro-scale strength σ_{micro} did not change, the observed changes of f and L may be the result of elastic rebound. Under a reduced load, elastic deformation of microstructures would be reduced, returning the structures to a state of less stress and strain, evident in increases in f and L, respectively.

Large significant changes in σ_{micro} indicate that this microstructural estimate may be a good indicator for changes in weak layer residual strength, which plays a large role in snowpack stability. When sampling thick weak layers that have recently experienced very large loading events, fewer profiles may be necessary to recognize changes in micro-structure than are needed for thin weak layers or small loading events. With an increased slab load, the difference in L between the slab and weak layer became more pronounced (ΔL increased), supporting previous findings by Pielmeier et al. (2006) and Pielmeier and Schweizer (2007).

4.2. Field method

This field technique is useful for obtaining microstructural estimates of existing stratigraphic features under varying loads. It also allows us to test how a potential weakness reacts to an artificial loading event, which may provide valuable information about how the snowpack will respond to new snowfall events. This allows us to broaden our datasets relating microstructure to slope instabilities even in the temporary absence of backcountry instabilities. This test could be efficiently used to obtain critical microstructural threshold values of many stratigraphic weaknesses. Such information may prove useful for establishing or testing SMP stability algorithms. The test can be applied over larger time frames as well, to deduce rates of strengthening or weakening. For near-surface instabilities, testing on flat terrain may be easier and allow for properties of the entire slab to be recorded.

As with standard isolated column tests, effects from column isolation may influence the results. Edge effects may result in microstructural information that is not pertinent to an intact *in situ* snowpack. Characterizing initial conditions of a weak layer within an isolated column, as well as the effects of column isolation, are difficult. Proper characterization may necessitate multiple profiles (Pielmeier and Marshall, 2009-this issue) which, in turn, would compromise the testable sampling extent. Increasing the column dimensions would increase the available sampling area, but would make column loading very difficult. Alternatively, recording multiple SMP profiles directly adjacent to (e.g. 10–15 cm peripheral to) the planned isolated columns would provide additional information about the initial conditions without compromising, or requiring use of, the available column sampling area. These additional profiles could be recorded before pit excavation, as well as into the prepared pit wall adjacent to the cut columns before altering their loads.

Despite these interesting results, the SMP and other penetrometers will not replace existing testing techniques, but will rather strengthen the diverse tools employed by researchers and practitioners. Haefeli, who developed the Ramsonde and recognized the potential of improving penetrometer technology (e.g. Bradley, 1966:260), warned of overrating any one observation type: "The factors determining avalanche danger are of such diverse nature, that each method which measures only one characteristic of the snowpack must be considered partial and therefore insufficient" (transl. Bader et al., 1939:150).

Acknowledgements

Thanks to Erich Peitzsch for field assistance and to Randy Spence and Moonlight Basin Ski Patrol for providing weather observations and site access, and for steering us toward undisturbed depth hoar late in the season. We also thank two anonymous reviewers and the Guest Editor for valuable comments that improved the paper. This research was supported in part by the U.S. National Science Foundation's Geography and Regional Science (Grant No. BCS-024310) and GK-12 Programs.

References

Bader, H.P., Haefeli, R., Bucher, E., Neher, J., Eckel, O. and Thams, C., 1939. Der Schnee und seine Metamorphose. Beitraege zur Geologie der Schweiz, Geotechnische Serie, Hydrologie Lieferung 3. Kümmerly and Frey, Zürich, 340 pp.
Birkeland, K., Kronholm, K., Schneebeli, M., Pielmeier, C., 2003. Temporal changes in the shear strength and hardness of a buried surface hoar layer. Ann. Glaciol. 38.
Bradley, C.D., 1966. The snow resistograph and slab avalanche investigations. International Symposium on Scientific Aspects of Snow and Ice Avalanches. April 5th–10th, 1965: Davos, Switzerland. International Union of Geodesy and Geophysics (IUGG) and International Association of Scientific Hydrology (IASH); Commission of Snow and Ice. Pub. No. 69.
Brown, R., Birkeland, K., 1990. A comparison of the digital resistograph with the ram penetrometer. Proceedings International Snow Science Workshop, Bigfork, MT, USA, pp. 19–30.
Chambers, J.M., Cleveland, W.S., Kleiner, B., Tukey, P.A., 1983. Graphical Methods for Data Analysis. Wadsworth and Brooks/Cole.
Colbeck, S.C., Akitaya, E., Armstrong, R., Gubler, H., Lafeuille, J., Lied, K., McClung, D., Morris, E., 1990. International classification for seasonal snow on the ground. International Commission for Snow and Ice (IAHS), World Data Center A for Glaciology. InUniversity of Colorado, Boulder, CO, USA.
DeQuervain, M., 1950. Die Festigekeitseigenschaften der Schneedecke und ihre Messung. Geofis. Pura Appl. 18, 15.
Dowd, T., Brown, R.L., 1986. A new instrument for determining strength profiles in snow cover. J. Glaciol. 32 (111), 299–301.
Fuller, R., 2004. Observations of an increase in slab thickness after fracture. Proceedings International Snow Science Workshop 2004, Jackson Hole, WY, USA, pp. 32–38.
Greene, E., Birkeland, K.W., Elder, K., Johnson, G., Landry, C., McCammon, I., Moore, M., Sharaf, D., Sterbenz, C., Tremper, B., Williams, K., 2004. Snow, weather, and avalanches: observational guidelines for avalanche programs in the United States. The American Avalanche Association. Pagosa Springs, CO.
Gubler, H., 1978. Determination of the mean number of bonds per snow grain and of the dependence of the tensile strength of snow on stereological parameters. J. Glaciol. 20 (83), 329–341.
Johnson, J., Schneebeli, M., 1999. Characterizing the micro-structural and micromechanical properties of snow. Cold Reg. Sci. Technol. 30, 91–100.
Kronholm, K., 2004. Spatial variability of snow mechanical properties with regard to avalanche formation. Doctoral dissertation. Mathematics and Natural Sciences Faculty, University of Zurich, Switzerland. pp. 187.
Lutz, E. 2009. Spatial and temporal analysis of snowpack strength and stability and environmental determinants on an inclined, forest opening. Doctoral dissertation. Department of Earth Sciences, Montana State University, Bozeman, MT. pp. 395.
Lutz, E., Birkeland, K.W., Kronholm, K., Hansen, K., Aspinall, R., 2007. Surface hoar characteristics derived from a snow micropenetrometer using moving window statistical operations. Cold Reg. Sci. Technol. 37 (3), 393–405.
Marshall, H.P. and Johnson, J., submitted for publication. Accurate inversion of snow micropenetrometer signals for microstructural and micromechanical properties. Journal of Geophysical Research - Earth Surface.
McClung, D.M., Schaerer, P., 1993. The Avalanche Handbook. The Mountaineers, Seattle.
McGill, R., Tukey, J.W., Larsen, W.A., 1978. Variations of box plots. Am. Stat. 32, 12–16.
Mellor, M., 1975. A review of basic snow mechanics. Snow Mechanics Symposium, International Association of Hydrological Sciences Publication No. 114, pp. 251–291.
Pielmeier, C., Schweizer, J., 2007. Snowpack stability information derived from the SnowMicroPen signal. Cold Reg. Sci. Technol. 47 (1), 102–107.
Pielmeier, C., Marshall, H.P., 2009. Rutschblock-scale snowpack stability derived from multiple quality-controlled SnowMicroPen measurements. Cold Reg. Sci. and Technol. 59, 178–184 (this issue).
Pielmeier, C., Marshall, H.P., Schweizer, J., 2006. Improvements in the application of the SnowMicroPen to derive stability information for avalanche forecasting. Proceedings International Snow Science Workshop 2006, Telluride CO, USA, pp. 187–192.

Schneebeli, M., Johnson, J., 1998. A constant-speed penetrometer for high-resolution snow stratigraphy. Ann. Glaciol. 26, 107–111.
Schneebeli, M., Pielmeier, C., Johnson, J., 1999. Measuring snow microstructure and hardness using a high resolution penetrometer. Cold Reg. Sci. Technol. 30 (1–3), 101–114.
Schweizer, J., 1999. Review of dry snow avalanches release. Cold Reg. Sci. Technol. 30 (1–3), 43–57.
Shapiro, L.H., Johnson, J.B., Sturm, M., Blaisdell, G.L., 1997. Snow mechanics: review of the state of knowledge and applications. CRREL Report 97-3. August 1997.
Yosida, Z., et al., 1956. Physical studies on deposited snow. II, Mechanical properties (#1). Contrib. Inst. Low Temp. Sci. 9, 1–81.